Simulation-based Calibration Approach to Large-area Phoswich Detectors for Simultaneous Alpha/Beta Detection

Wooseub Kim [a], Jinhwan Kim [a], Junhyeok Kim [a], Sopan Das [a], Minhwan Kim [a], Eunbi Ko [a] and Gyuseong Cho [a*]
[a]*Dept of Nuclear and Quantum Engineering, Korea Advanced Institute of Science and Technology, Daejeon 291*
[*]*Corresponding author: gscho1@kaist.ac.kr*

1. Introduction

Kori unit 1, the first commercial nuclear power plant (NPP) in Korea, was determined to be shut down permanently in June 2017. Decommissioning activities will be mainly implemented after 2022 [1]. Globally, 183 NPP units are expected to retire in the 2020s [2]. In this aspect, decommissioning old NPPs is an inevitable issue.

In decommissioning, the radiological characterization of potentially contaminated sites is required to estimate the residual radioactivity. Prior to actual samplings for the analysis, scanning survey with a movable radiation detector enables to measure the contaminated sites quickly and find local areas with elevated activity [3].

For the scanning survey, minimum detectable concentration (MDC) of a field survey instrument is an important factor to reliably measure radiation particles and verify whether the contaminated sites exceed residual radioactivity criteria. The MDC is directly affected by instrument efficiency, which is determined by parameters such as probe surface area, source-to-detector geometry, radiation type and radionuclide energy [3, 4].

In this research, large-area phosphor sandwich (Phoswich) detectors for simultaneous alpha and beta detection were manufactured to identify instrument efficiency variations with the probe areas of $100 \times 100\ mm^2$, $150 \times 150\ mm^2$ and $200 \times 200\ mm^2$. Instrument calibration was conducted with the limited sizes of radioactive sources compared to the probe areas. To achieve the same effects of source-to-detector geometry with the same probe areal radioactive source, new instrument calibration approach was conducted based on the simulation results of Monte Carlo N-Particle Transport Code (MCNP).

2. Materials and methods

2.1. Experimental details

The designed phoswich detector consists of 6 μm thick aluminized mylar, 80 μm thick ZnS:Ag (Eljen, EJ-600), 0.25 mm thick plastic scintillator (Eljen, EJ-212), light guide and photomultiplier tube (PMT) of 3-inch photocathode diameter (Hamamatsu photonics, R6233). Optical grease (Saint-Gobain, BC-630) was used to remove an air gap at contact areas and minimize the loss of optical photons emitted from scintillators.

Polymethyl methacrylate (PMMA) light guides were prepared to enhance the light collection efficiency of optical photons. Light guides of 10 mm, 20 mm and 30 mm thickness were coupled to $100 \times 100\ mm^2$ probe areal phoswich detector. Likewise, Light guides of 15 mm, 30 mm and 40 mm thickness were coupled to $150 \times 150\ mm^2$ and $200 \times 200\ mm^2$ probe areal phoswich detectors. Teflon (PTFE) tape was covered on the side of light guides to prevent the escape of optical photons and reflect it.

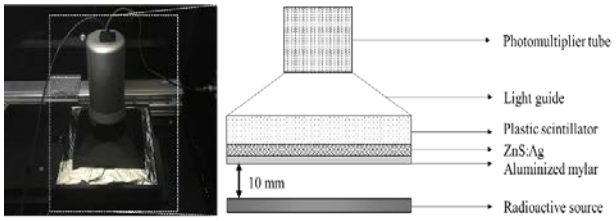

Fig. 1. The description of the phoswich detector for simultaneous alpha and beta detection.

To measure alpha and beta rays from radioactive sources, a digitizer (Caen, DT5725) was connected to the phoswich detector and digitized PMT anode pulses for pulse shape discrimination (PSD). All experiments were conducted under the background radiation level of 10 μR/hr and inside of a dark box. In any case, background count rates were measured as less than 300 cpm.

2.2. MCNP simulation for calibration approach

The detector response is critically influenced by radiation type, radionuclide energy and source-to-detector geometry. However, the actual dimension of a potentially contaminated area can not be known *a priori*. It may be appropriate to use an instrument efficiency calibrated from a distributed source for all surface activity measurements except localized areas of elevated activity because it is a long process to determine a specific contaminant geometry during the scanning [3, 5].

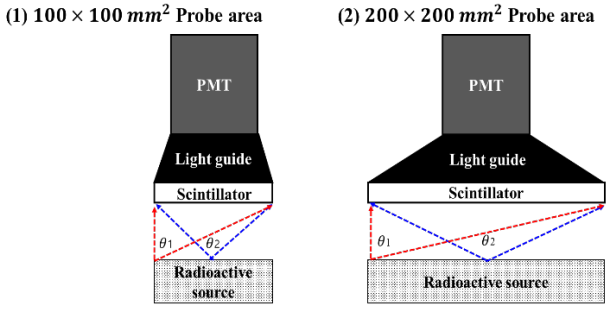

Fig. 2. A schematic of source-to-detector geometries depending on the probe areas of (1) $100 \times 100\ mm^2$, and (2) $200 \times 200\ mm^2$.

Fig. 2 shows the source-to-detector geometries depending on probe areas. As probe area increases, source-detector geometrical efficiency grows. To define overall instrument efficiency by considering the geometrical efficiency, the same probe areal radioactive source is ideally required.

In this research, 150×100 mm^2 areal Am-241 alpha source and 100×100 mm^2 areal SrY-90 beta source were used for instrument calibration. The sizes of the radioactive sources were not well-matched with the probe areas. To overcome this limitation and achieve the same effects as using the same probe areal radioactive sources, the vertically and horizontally symmetric feature of probe areas was used.

When a probe areal radioactive source is positioned under the probe of a phoswich detector, radiation interactions will occur at the entire probe area. In this case, it can be assumed that the four radioactive sources of the 1/4 probe area are placed one another under the probe. Radiations coming out from each 1/4 probe areal source will interact at the probe. The patterns of radiation energy deposition at a certain location of the probe will be the same because of the symmetric characteristic.

To prove that this assumption is correct, MCNP 6.2 simulations were performed. In the simulated geometry for radiation transport, a probe was implemented as a 0.33 mm thick phoswich scintillators composed of 0.08 mm thick ZnS:Ag layer and 0.25 mm thick plastic scintillator. The entire volume of each probe was divided into small voxels of $10 \times 10 \times 0.33$ mm^3 to determine where radiation particles mostly deposit energies at the probe. Dry air was assumed as the surrounding material. Am-241 and SrY-90 radioactive source inputs were entered based on the nuclear decay data of ICRP Publication 107.

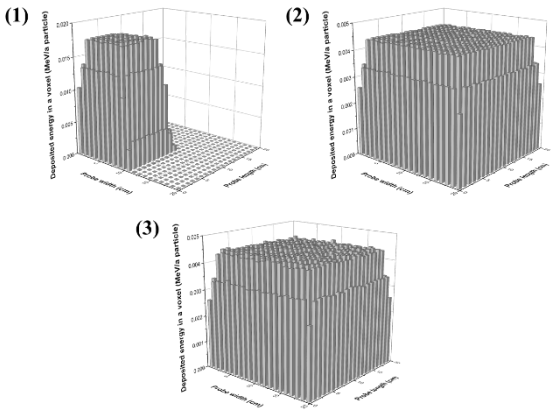

Fig. 3. (1) Energy deposition trend with the 1/4 probe areal Am-241 source, (2) symmetrically duplicated energy deposition trend with the 1/4 probe areal Am-241 source, and (3) energy deposition trend with the same probe areal Am-241 source.

Fig. 3(1) shows the deposited energy in each voxel (MeV/a particle) when the 1/4 probe areal Am-241 source is located under the corner of 200×200 mm^2 areal probe. Fig. 3(2) shows that the deposited energy result of Fig. 3(1) is duplicated symmetrically at where radioactive sources were not positioned, and then the summation of the deposited energy in each voxel from the four duplicated Am-241 sources of the 1/4 probe area was averaged. Fig. 3(3) shows that the deposited energy in each voxel with the same probe areal Am-241 source.

The simulation results showed that Fig. 3(2) and Fig. 3(3) are nearly the same in terms of total deposited energy and locations where radiation particles mostly deposit energies. In the case of a 1/2 probe areal source as well as SrY-90 beta source, the same tendency was observed in MCNP simulation results.

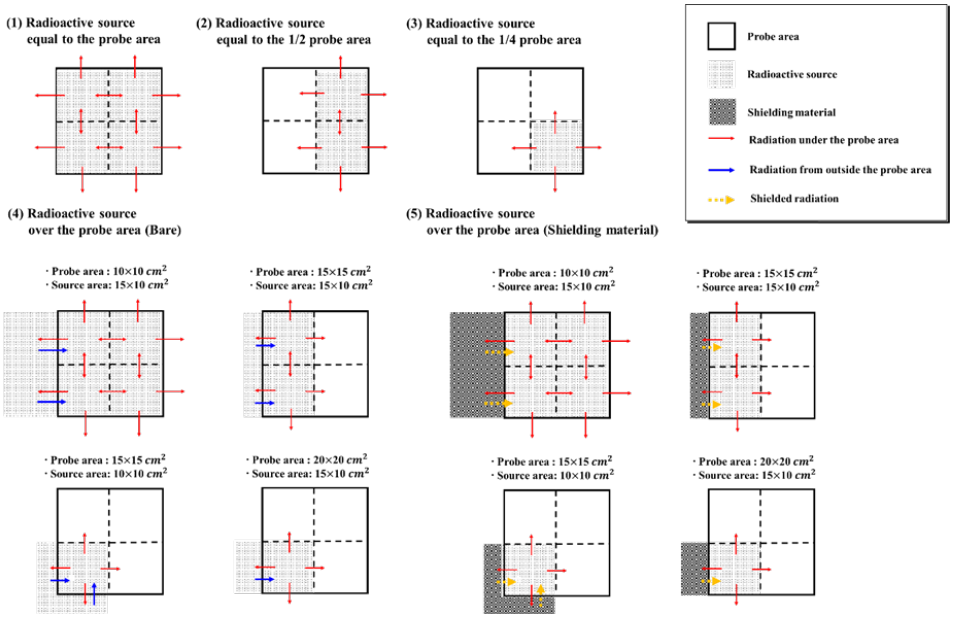

Fig. 4. Possible scenarios of positioning a radioactive source (1) equal to the probe area, (2) equal to the 1/2 probe area, (3) equal to the 1/4 probe area, (4) over the probe area without a shielding material, and (5) over the probe area with a shielding material.

Thus, if a 1/4 probe areal source, a 1/2 probe areal source and an entire probe areal source have the same surface emission rate, total deposited energy at the probe during the same time will be similar. As proved by the energy deposition trends in Fig. 3, optical photons emitted from a certain area of the phoswich scintillator due to radiation energy deposition will have the same light collection probabilities to contribute to counting measurements. In other words, calibrated instrument efficiency will be the same.

Fig. 4(4) shows possible scenarios to locate $150 \times 100\ \mathrm{mm}^2$ areal Am-241 alpha source and $100 \times 100\ \mathrm{mm}^2$ areal SrY-90 beta source under a probe for instrument calibration. Some part of source areas can be located outside a probe. Without a shielding material, radiations from outside the probe area can contribute to total energy deposition. It will cause that instrument efficiency is overestimated. According to MCNP simulation results, 1 mm thick lead could effectively shield radiations from outside the probe area. Therefore, a 1 mm thick lead was used for instrument calibration.

Corrected surface emission rate was used to calculate instrument efficiency by following the equation (1).

$$q_{2\pi} = q_{2\pi,act}\left(\frac{A_p}{A_s}\right), \quad (1)$$

Where $q_{2\pi}$ is the corrected surface emission rate of a radioactive source in dpm, $q_{2\pi,act}$ is the actual surface emission rate of a radioactive source in dpm, A_s is the total area of a radioactive source, and A_p is the source area within the probe.

2.3. Instrument efficiency

Instrument response can be converted to the residual activities of potentially contaminated sites. Calibration sources are recommended to have similar features of the contaminated sites.

Instrument efficiency stands for a ratio of the net count rates of an instrument to the surface emission rate of a radioactive source in a particular geometry. The surface emission rate means the number of radiation particles coming out from the front surface of a radioactive source per unit time. Instrument efficiency (ε_i) and the uncertainty of the instrument efficiency (σ_i) were derived by the following equation (2, 3) [5].

$$\varepsilon_i = \frac{C_{S+B} - C_B}{q_{2\pi}}, \quad (2)$$

$$\sigma_i = \varepsilon_i \sqrt{\left(\frac{\sqrt{\sigma_{S+B}^2 + \sigma_B^2}}{C_{S+B} - C_B}\right)^2 + \left(\frac{\sigma_{2\pi}}{q_{2\pi}}\right)^2}, \quad (3)$$

Where C_{S+B} is the gross count rate of the measurement in cpm, C_B is the background count rate in cpm, $q_{2\pi}$ is the surface emission rate of a radioactive source in dpm, σ_{S+B} is the uncertainty of gross count rate in cpm, σ_B is the uncertainty of background count rate in cpm, and $\sigma_{2\pi}$ is the uncertainty of the surface emission rate in dpm.

The instrument efficiencies of Am-241 and SrY-90 were determined by experimental data. Gross count rates and background count rates were measured five times for 15 minutes.

3. Results and discussion

Fig. 5 shows instrument efficiency variations depending on the thickness of light guides. The instrument efficiencies were the highest when the thickness of a light guide is 20 mm for $100 \times 100\ \mathrm{mm}^2$ areal probe, 30 mm for $150 \times 150\ \mathrm{mm}^2$ areal probe and 30 mm for $200 \times 200\ \mathrm{mm}^2$ areal probe. The difference of instrument efficiencies occurs due to the change in light collection efficiency.

Table I summarizes the instrument efficiencies of large-area phoswich detectors when counting measurements are the best.

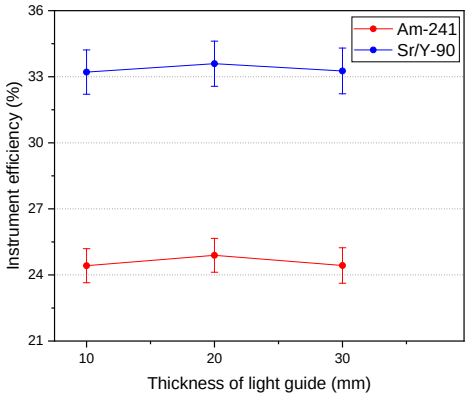

(1)

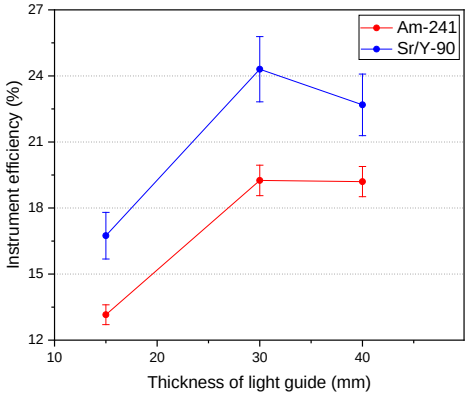

(2)

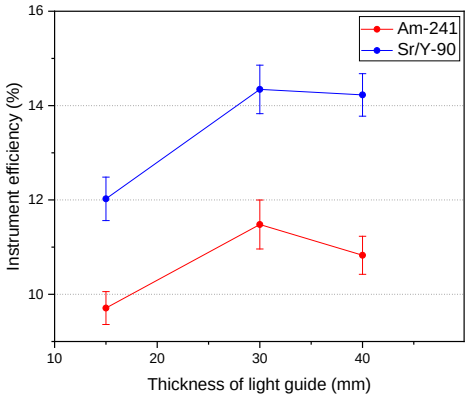

(3)

Fig. 5. Instrument efficiency variations depending on the thickness of light guides coupled to the probe areas of (1) 100×100 mm^2, (2) 150×150 mm^2, and (3) 200×200 mm^2.

Table I: The instrument efficiencies of large-area phoswich detectors.

Probe area (mm^2)	**Radioactive source**	**Instrument efficiency (%)**
100×100	Am-241	24.892 ± 0.767
	SrY-90	33.592 ± 1.026
150×150	Am-241	19.254 ± 0.691
	SrY-90	24.304 ± 1.481
200×200	Am-241	11.481 ± 0.519
	SrY-90	14.344 ± 0.514

4. Conclusion

In this research, large-area phoswich detectors for simultaneous alpha and beta detection were manufactured to identify instrument efficiency variations with probe areas, which affect the MDC of a field survey instrument. For instrument calibration, the limited sizes of Am-241 and SrY-90 sources compared to the probe areas were used. To achieve the same effects of source-to-detector geometries with the same probe areal radioactive sources, new simulation-based calibration approach was conducted. In this approach, 1 mm thick lead worked well as a shielding material for instrument calibration. It was confirmed that instrument efficiency can be enhanced by using an optimal light guide. Experimental results showed that instrument efficiencies for the radionuclides decrease as the probe area increases.

For further study, other radioactive sources will be used to estimate instrument efficiencies for other radionuclides. Based on the experimental results, static MDC and scan MDC will be derived and compared to examine the MDC variations with probe areas.

5. Acknowledgements

This work was supported by the Nuclear Research & Development Program of the National Research Foundation of Korea (NRF) grant funded by the Ministry of Science, ICT and Future Planning (MISP) (Grant code: 2017M2A2A6A02020807, 2018M2A8A5023361).

This work was partly supported by a National Research Foundation of Korea (NRF) grant funded by the Korean government (MSIP) (NRF-2017M2A8A50 15084).

REFERENCES

[1] H. W. Seo, W. Sohn, K. H. Jo, Proposal for the spent nuclear fuel management plan from the decommissioning of Kori site NPPs, Annals of Nuclear Energy, Vol.120, pages 749-762, 2018.

[2] Mordor Intelligence LLP, Global Nuclear Decommissioning Market –Growth, Trends and Forecast (2018-2023), 2018.

[3] U.S. Nuclear Regulatory Commission, Multi-Agency Radiation Survey and Site Investigation Manual (MARSSIM), NRC; NUREG-1575, Rev. 1, 2000.

[4] E. W. Abelquist, Decommissioning Health Physics: A Handbook for MARSSIM Users, 2nd edition, 2013.

[5] U.S. Nuclear Regulatory Commission, Minimum Detectable Concentrations With Typical Radiation Survey Instruments for Various Contaminants and Field Conditions, NUREG-1507, 1998.